Biomedical Optics EXPRESS

Terahertz imaging of excised oral cancer at frozen temperature

Yookyeong Carolyn Sim,[1,5] Jae Yeon Park,[2,5] Kang-Min Ahn,[3] Chansik Park,[4] and Joo-Hiuk Son[2,*]

[1] *Department of Physics, Princeton University, New Jersey 08544, USA*
[2] *Department of Physics, University of Seoul, Seoul 130-743, South Korea*
[3] *Department of Oral and Maxillofacial Surgery, Asan Medical Center, Seoul 138-736, South Korea*
[4] *Department of Histology, Asan Medical Center, Seoul 138-736, South Korea*
[5] *These authors contribute equally to this paper*
** joohuik@uos.ac.kr*

Abstract: The feasibility of terahertz (THz) imaging at frozen temperature for the clinical application of oral cancer detection was investigated by analyzing seven oral tissues resected from four patients. The size, shape, and internal position of the oral cancers were mapped by THz radiation in the frequency range of 0.2–1.2 THz at –20 °C and 20 °C, and compared with those identified in the histological examination. THz imaging of frozen tissue was found to offer greater sensitivity in distinguishing cancerous areas from surrounding tissue and a larger THz-frequency spectral difference between the oral cancer and normal mucosa than room-temperature THz imaging. A cancerous tumor hidden inside tissue was also detected using this method by observing the THz temporal domain waveform. The histological analysis showed that these findings resulted from cell structure deformations involving the invasion of oral tumor and neoplastic transformations of mucous cells. Therefore, a cytological approach using THz radiation at a frozen temperature might be applied to detect oral cancer.

OCIS codes: (170.3880) Medical and biological imaging; (160.1435) Biomaterials; (040.2235) Far infrared or terahertz; (110.6795) Terahertz imaging; (300.6495) Spectroscopy, terahertz.

References and links

1. B. W. Neville and T. A. Day, "Oral cancer and precancerous lesions," CA Cancer J. Clin. **52**(4), 195–215 (2002).
2. S. Warnakulasuriya, "Global epidemiology of oral and oropharyngeal cancer," Oral Oncol. **45**(4-5), 309–316 (2009).
3. P. E. Petersen, "Oral cancer prevention and control--the approach of the World Health Organization," Oral Oncol. **45**(4-5), 454–460 (2009).
4. I. Ganly, S. Patel, and J. Shah, "Early stage squamous cell cancer of the oral tongue--clinicopathologic features affecting outcome," Cancer **118**(1), 101–111 (2012).
5. S. E. Scott, E. A. Grunfeld, and M. McGurk, "The idiosyncratic relationship between diagnostic delay and stage of oral squamous cell carcinoma," Oral Oncol. **41**(4), 396–403 (2005).
6. S. Ram and C. H. Siar, "Chemiluminescence as a diagnostic aid in the detection of oral cancer and potentially malignant epithelial lesions," Int. J. Oral Maxillofac. Surg. **34**(5), 521–527 (2005).
7. E. S. Oh and D. M. Laskin, "Efficacy of the vizilite system in the identification of oral lesions," J. Oral Maxillofac. Surg. **65**(3), 424–426 (2007).
8. D. C. De Veld, M. J. Witjes, H. J. Sterenborg, and J. L. Roodenburg, "The status of in vivo autofluorescence spectroscopy and imaging for oral oncology," Oral Oncol. **41**(2), 117–131 (2005).
9. D. Roblyer, R. Richards-Kortum, K. Sokolov, A. K. El-Naggar, M. D. Williams, C. Kurachi, and A. M. Gillenwater, "Multispectral optical imaging device for in vivo detection of oral neoplasia," J. Biomed. Opt. **13**(2), 024019 (2008).
10. E. Pickwell and V. P. Wallace, "Biomedical applications of terahertz technology," J. Phys. D Appl. Phys. **39**(17), 301–310 (2006).

#190896 - $15.00 USD Received 24 May 2013; revised 16 Jul 2013; accepted 16 Jul 2013; published 23 Jul 2013

11. T. R. Globus, D. L. Woolard, T. Khromova, T. W. Crowe, M. Bykhovskaia, B. L. Gelmont, J. Hesler, and A. C. Samuels, "THz-spectroscopy of biological molecules," J. Biol. Phys. **29**(2/3), 89–100 (2003).
12. J.-H. Son, "Terahertz electromagnetic interactions with biological matter and their applications," J. Appl. Phys. **105**(10), 102033 (2009).
13. J. Y. Park, H. J. Choi, K.-S. Cho, K.-R. Kim, and J.-H. Son, "Terahertz spectroscopic imaging of a rabbit VX2 hepatoma model," J. Appl. Phys. **109**(6), 064704 (2011).
14. S. Sy, S. Huang, Y.-X. Wang, J. Yu, A. T. Ahuja, Y.-T. Zhang, and E. Pickwell-MacPherson, "Terahertz spectroscopy of liver cirrhosis: investigating the origin of contrast," Phys. Med. Biol. **55**(24), 7587–7596 (2010).
15. S. J. Oh, J. Y. Kang, I. H. Maeng, J.-S. Suh, Y.-M. Huh, S. J. Haam, and J.-H. Son, "Nanoparticle-enabled terahertz imaging for cancer diagnosis," Opt. Express **17**(5), 3469–3475 (2009).
16. S. J. Oh, J. H. Choi, I. H. Maeng, J. Y. Park, K. G. Lee, Y.-M. Huh, J.-S. Suh, S. J. Haam, and J.-H. Son, "Molecular imaging with terahertz waves," Opt. Express **19**(5), 4009–4016 (2011).
17. J. Y. Park, H. J. Choi, G.-E. Nam, K.-S. Cho, and J.-H. Son, "In vivo dual-modality terahertz/magnetic resonance imaging using superparamagnetic iron oxide nanoparticles as a dual contrast agent," IEEE Trans. THz Sci. Technol. **2**(1), 93–98 (2012).
18. J.-H. Son, "Principle and applications of terahertz molecular imaging," Nanotechnology **24**(21), 214001 (2013).
19. E. Pickwell, B. E. Cole, A. J. Fitzgerald, M. Pepper, and V. P. Wallace, "In vivo study of human skin using pulsed terahertz radiation," Phys. Med. Biol. **49**(9), 1595–1607 (2004).
20. R. M. Woodward, B. E. Cole, V. P. Wallace, R. J. Pye, D. D. Arnone, E. H. Linfield, and M. Pepper, "Terahertz pulse imaging in reflection geometry of human skin cancer and skin tissue," Phys. Med. Biol. **47**(21), 3853–3863 (2002).
21. B. E. Cole, R. M. Woodward, D. A. Crawley, V. P. Wallace, D. D. Arnone, and M. Pepper, "Terahertz imaging and spectroscopy of human skin in vivo," Proc. SPIE **4276**, 1–10 (2001).
22. A. J. Fitzgerald, V. P. Wallace, M. Jimenez-Linan, L. Bobrow, R. J. Pye, A. D. Purushotham, and D. D. Arnone, "Terahertz pulsed imaging of human breast tumors," Radiology **239**(2), 533–540 (2006).
23. Y. B. Ji, E. S. Lee, S.-H. Kim, J.-H. Son, and T.-I. Jeon, "A miniaturized fiber-coupled terahertz endoscope system," Opt. Express **17**(19), 17082–17087 (2009).
24. G. M. Png, J. W. Choi, B. W. Ng, S. P. Mickan, D. Abbott, and X.-C. Zhang, "The impact of hydration changes in fresh bio-tissue on THz spectroscopic measurements," Phys. Med. Biol. **53**(13), 3501–3517 (2008).
25. J. Nishizawa, T. Sasaki, K. Suto, T. Yamada, T. Tanabe, T. Tanno, T. Sawai, and Y. Miura, "THz imaging of nucleobases and cancerous tissue using a GaP THz-wave generator," Opt. Commun. **244**(1-6), 469–474 (2005).
26. S. G. Fitzpatrick, A. N. Neuman, D. M. Cohen, and I. Bhattacharyya, "The clinical and histologic presentation of gingival squamous cell carcinoma: a study of 519 cases," Oral Surg Oral Med Oral Pathol Oral Radiol **114**(4), 509–515 (2012).
27. J. P. Shah and Z. Gil, "Current concepts in management of oral cancer--surgery," Oral Oncol. **45**(4-5), 394–401 (2009).
28. R. W. Chan and I. R. Titze, "Effect of postmortem changes and freezing on the viscoelastic properties of vocal fold tissues," Ann. Biomed. Eng. **31**(4), 482–491 (2003).
29. M. Geerligs, G. W. Peters, P. A. Ackermans, C. W. Oomens, and F. P. Baaijens, "Linear viscoelastic behavior of subcutaneous adipose tissue," Biorheology **45**(6), 677–688 (2008).
30. G. A. Kim, H. Y. Kim, J. W. Kim, G. Lee, E. Lee, J. Y. Ahn, J. H. Park, and J. M. Lim, "Effectiveness of slow freezing and vitrification for long-term preservation of mouse ovarian tissue," Theriogenology **75**(6), 1045–1051 (2011).
31. A. Z. Higgins, D. K. Cullen, M. C. LaPlaca, and J. O. Karlsson, "Effects of freezing profile parameters on the survival of cryopreserved rat embryonic neural cells," J. Neurosci. Methods **201**(1), 9–16 (2011).
32. M. Szarko, K. Muldrew, and J. E. Bertram, "Freeze-thaw treatment effects on the dynamic mechanical properties of articular cartilage," BMC Musculoskelet. Disord. **11**(1), 231 (2010).
33. P. N. Nonaka, N. Campillo, J. J. Uriarte, E. Garreta, E. Melo, L. V. de Oliveira, D. Navajas, and R. Farré, "Effects of freezing/thawing on the mechanical properties of decellularized lungs," J. Biomed. Mater. Res. A (to be published).

1. Introduction

Oral cancer is a major worldwide public health issue. There are over 400,000 new cases every year, and in half of the cases, the patient is given a survival estimate of less than five years. Cancer development is preceded by visible mucosal changes, and its major risk factors include smoking, alcohol, smokeless tobacco, and human papilloma virus [1]. Over the last 50 years, almost 90% of oral cancer cases have been squamous cell carcinomas [2–4].

Despite recent advances in detection and treatment, oral cancer still carries a high mortality rate, higher than that of liver, kidney, brain, or skin cancers. This is because of the high rate of metastasis to other locations, which happens when a cancerous tumor is routinely found in later stages. Because of its asymptomatic nature, oral cancer cannot be easily detected in its early stages, and therefore carries a high risk of secondary tumor. The detection

#190896 - $15.00 USD Received 24 May 2013; revised 16 Jul 2013; accepted 16 Jul 2013; published 23 Jul 2013

of oral cancer in its early stages leads to significantly reduced mortality and morbidity [5]. Therefore, there is a great demand for a non-invasive method for early-stage screening of cancerous changes. Better targeted diagnostic testing could systematically reduce the overall cost and time of treatment. New diagnostic aids to conventional oral examinations have been recently introduced to assist in the early detection of oral cancer [6–9].

Terahertz (THz) imaging, which utilizes the electromagnetic radiation spectrum between 0.1 and 10 THz, has been investigated to assess its potential to diagnose cancers by measuring the water content change and cell deformation of malignant tumors [10–14] or by sensing the nanoparticle probes targeted at cancerous tumors [15–18]. Those applications have mainly focused on skin and breast cancers because THz radiation cannot penetrate deep into skin because of its high absorption by water in tissue [19–22]. A newly developed miniaturized THz endoscope has expanded the applicability of the THz imaging technique to cancers in other organs [23]. Oral cancer could be a good candidate for diagnosis by THz endoscopic imaging.

The increase of water amount in tumor coming from the rapid growth of vessels around cancerous cells contributes to the contrast mechanism of THz imaging for cancer diagnosis, but the water in the tissue limits the permeability of the THz wave to only measure the surface tissue, which results in less interaction between the THz wave and the tissue. This can be circumvented by lowering the hydration level of fresh tissues [24]. One of dehydration technique is lyophilization, which is a dry freezing method performed regularly in clinical trials. In this study, frozen oral tissues with cancer have been imaged using THz radiation and compared with the results of room-temperature THz measurement, as well as with histological images.

2. Experiments

Seven oral tumors, sized about 1 cm^2, were obtained with palpation during surgery from the tongue, palate, and attached gingiva of four patients (Fig. 1). The surgeon diagnosed the cancer types as mucoepidermoid carcinoma and squamous cell carcinoma, as listed in Table 1. The freshly excised specimens were immediately frozen on dry ice to preserve their fresh state and then imaged using THz radiation at –20 °C and 20 °C in sequence before histological processing. After THz imaging, the samples were fixed in a formalin solution to preserve the cell structure and dyed with hematoxylin and eosin staining. The cancerous area was identified by histopathological examination of vertical or horizontal sections at the Department of Pathology, Asan Medical Center. The Asan Medical Center Institutional Review Board approved this study (Institutional Review Board study No. 2011-0421).

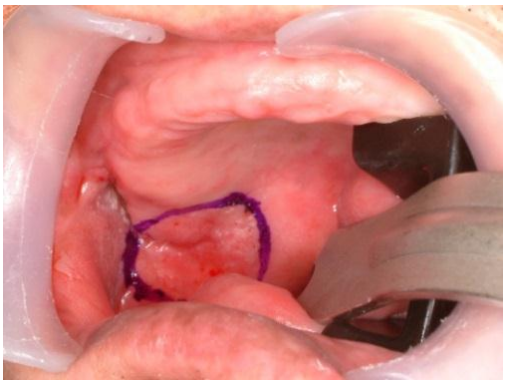

Fig. 1. Oral cancer diagnosis in the operating room. The cancer is located on the lateral surface of the tongue and a safety margin of 1.5 cm is marked.

#190896 - $15.00 USD Received 24 May 2013; revised 16 Jul 2013; accepted 16 Jul 2013; published 23 Jul 2013

Table 1. Table of tissue sample categories (MEC: mucoepidermoid carcinoma, SCC: squamous cell carcinoma).

Identification	*Cancer*	*Cancer Type*
#1	Y	MEC
#2	Y	MEC
#3	Y	SCC
#4	Y	SCC
#5	Y	SCC
#6	Y	SCC
#7	Y	SCC

All oral specimens were measured by using a reflection-type THz imaging system with a temperature-controllable sample chamber as shown in Fig. 2. The specimens and an aluminum film were mounted on a quartz substrate in a chamber that was sealed to maintain a specified temperature using a gas pump. The aluminum film was used to acquire a reference signal of a THz time-domain waveform by reflection. The recorded THz pulses were used to calculate the THz absorption and refractive index in the frequency range of 0.2–1.2 THz. The full data of a THz image were collected in raster scan mode with a step of 0.25 mm, and each image pixel was represented by the real part of the THz refractive indices.

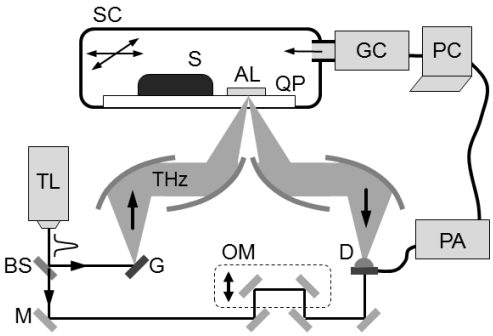

Fig. 2. THz imaging setup for detecting oral cancer at –20 °C and 20 °C. The setup is designed in reflection mode and the sealed chamber is utilized to control the temperature inside. The aluminum film in the chamber is used to reflect the reference signal. (SC: sealed chamber, S: specimen, AL: aluminum film, QP: quartz plate, GC: gas controller, TL: Ti:sapphire laser, BS: beam splitter, M: mirror, G: THz generator, THz: THz radiation, OM: oscillating mirror, D: THz detector, PA: preamplifier)

3. Results

The seven oral samples obtained from Asan Medical Center were imaged by THz radiation and compared with histopathologic examination results. In the histological analyses, cancerous areas were identified on the surface of six samples and in the interior of the seventh sample. In Fig. 3, the image table of the six samples shows the optical image in column (a), and the frozen and room temperature THz images in columns (b) and (c), respectively, and the histological image in column (d). The images in columns (a), (c) and (d) were acquired at room temperature, but as the THz images in column (b) were recorded at –20 °C, their tissue sizes were slightly shrunken. The optical images of the specimens in column (a) show the color of blood, but no distinct signs of cancer. THz images in columns (b) and (c) are constructed with image pixels using a rainbow color map corresponding to the refractive indices at 0.5 THz. The green and yellow pixels are distributed in the tissues of all THz images, but groups of purple pixels are shown mostly in THz images of frozen tissues. The

#190896 - $15.00 USD Received 24 May 2013; revised 16 Jul 2013; accepted 16 Jul 2013; published 23 Jul 2013

purple groups in column (b) are correlated with the blue-lined cancerous areas on the histological images in column (d).

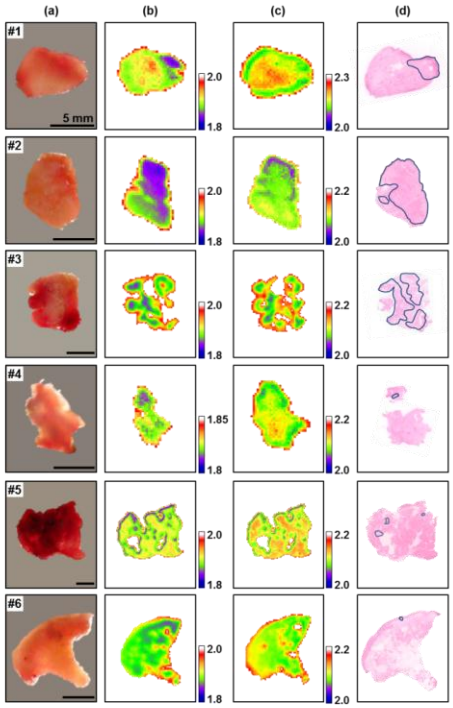

Fig. 3. (a) Optical images, (b) frozen and (c) room temperature THz images, and (d) histopathological images of six oral samples. THz images are displayed by the index of refraction at 0.5 THz, and the cancerous areas are marked with blue loops in the histological images.

Figure 4 shows a quantitative correlation of the cancerous area between the histological images and the THz images of the frozen specimens in Fig. 3. The area ratio was used as a correlation factor to define the cancerous area on the histological image (or the purple area located within the index range of 1.8 to 1.85 on the THz image of frozen tissue) for the whole size of the sample on both images.

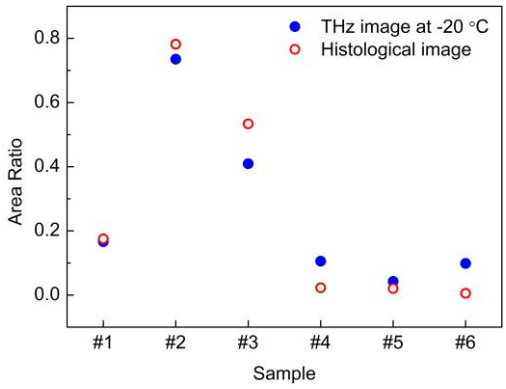

Fig. 4. The correlation of cancerous areas from THz imaging at –20 °C and histological imaging. The correlation factor is the area ratio of the whole size of specimen and the cancerous area (or purple area) within it on both images.

#190896 - $15.00 USD Received 24 May 2013; revised 16 Jul 2013; accepted 16 Jul 2013; published 23 Jul 2013

According to pathological analysis, cell structural features were found in and around the cancerous area, but there was no significant tissue damage or necrosis in the normal or cancer cells from the freezing and thawing process. As shown in Fig. 5(a), enlarged nuclei with hyperchromatism and pleomorphic cells with intercellular bridges were identified in the cancerous areas. These changes in cellular structure were originated by hypermitosis that increases the number of cells with abnormal shape and hyperchromatic nuclei. Surrounding tumor clusters, significant inflammatory host responses were found. Figures 5(b) and 5(c) show tissue damage caused by the proliferation of lymphocytes, macrophages and spindle cells, and the infiltration of some larger, eosinophilic and polygonal cells in the squamous cell epithelium. This supports that the purple groups in the THz images of frozen tissues originated from the interaction of the cellular structure with THz radiation.

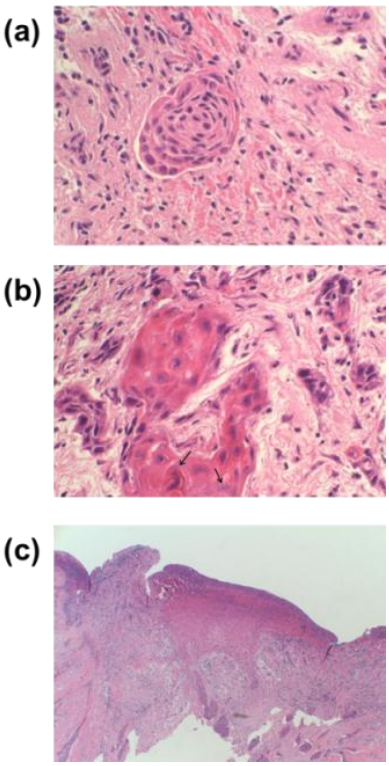

Fig. 5. (a) A nest of deformed mucosal cells with hyperchromatic nuclei from sample #1 (× 400), (b) a mixture of inflammatory cells from sample #2 (× 400), (c) mucoepidermoid carcinoma of the tongue showing subepithelial invasion from sample #1 (× 40).

We calculated the THz refractive index and absorption of oral cancer and normal mucosa to investigate the interaction between the cellular structure and THz radiation. The recorded THz reflection signals of the specimens and the aluminum film were transformed to the complex refractive index $\tilde{n}(\omega)$ in the frequency domain of 0.2–1.2 THz. The refractive index in the real part n(ω) and the absorption in the imaginary part α(ω) of the complex index $\tilde{n}(\omega)$ were obtained using the following equations:

$$\tilde{n}(\omega) = \mathrm{n} + \mathrm{i}\,\kappa = \frac{\sqrt{(1-r)^2 n_q^2 + 4r\sin\varphi}}{1-r}. \quad (1)$$

$$\alpha(\omega) = \frac{2\kappa\omega}{c}. \quad (2)$$

#190896 - $15.00 USD Received 24 May 2013; revised 16 Jul 2013; accepted 16 Jul 2013; published 23 Jul 2013

where κ is the extinction coefficient related to the absorption α, r is the reflection coefficient, n_q is the refractive index of the quartz substrate, φ is the incident angle, ω is the angular frequency and c is the speed of light in a vacuum. The THz refractive index and the absorption of oral cancer and normal mucosa at two temperatures are presented in Fig. 6. The circular and triangular dots in the spectra represent average values, and the error bars represent the 95% confidence interval. At room temperature, the average values of THz spectra in oral cancer are smaller than those in mucosa, and their error bars overlapped. The trend of their THz indices and absorption spectra is close to that of liquid water. This indicates that THz radiation has responded mostly to the liquid water in the tissues. The THz spectra at frozen temperatures follow those of ice, however, and have distinguishable gaps between normal mucosa and oral cancer in the frequency range of 0.5 to 1 THz. THz radiation is not absorbed by ice as strongly as liquid water, yet is affected by differences in cellular structure.

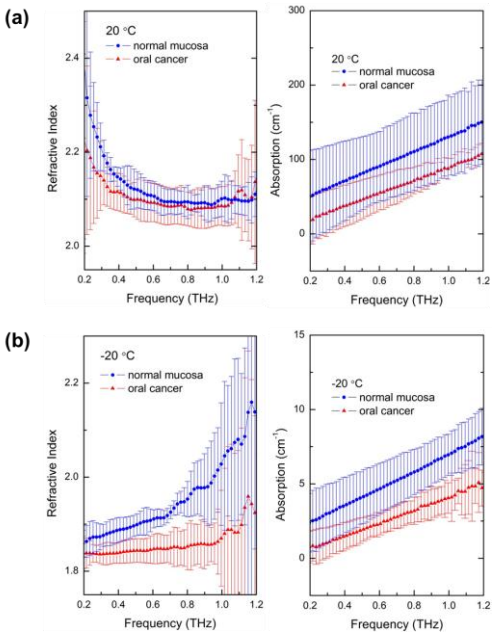

Fig. 6. The THz refractive indices and absorptions of normal mucosa and oral cancer of the six oral samples at (a) 20 °C and (b) –20 °C in the frequency range of 0.2–1.2 THz. The dots are the average values and the error bars represent the 95% confidence interval.

The differences in cellular structure between oral cancer and normal mucosa made it possible to detect the cancer below the tissue surface using pulsed THz radiation. An optical image, THz images taken at two temperatures, a histological image, and the THz time-domain signals of the seventh sample are shown in Fig. 7. The images in Figs. 7(a), 7(b), and 7(c) did not reveal any sign of cancer from surface measurements. The cancerous area was discovered during the histological examination from horizontal sectioning at the dashed line in Fig. 7(a). Figure 7(d) depicts the cancerous area that was located 1.3 mm from the quartz substrate. This distance can also be estimated by the THz optical path length as the THz radiation penetrated the mucosa tissue. THz time-domain waveforms acquired at the red arrows in Figs. 7(b) and 7(c) are presented in Fig. 7(e). The first pulses reflected from the interface between the quartz substrate and tissue surface were observed at both temperatures, but the second pulse, delayed by 17 ps, was discovered only at the frozen temperature. Considering the refractive index of frozen tissue and the incident angle of the focused THz beam, the optical distance calculation yielded 1.2 mm. The error of the optical distance calculation is about 0.1

#190896 - $15.00 USD Received 24 May 2013; revised 16 Jul 2013; accepted 16 Jul 2013; published 23 Jul 2013

mm, and its major reason might be because of tissue shrinkage at frozen temperatures. THz imaging using the freezing technique measured the exact location of cancers below 1 mm by distinguishing the differences in cell structure.

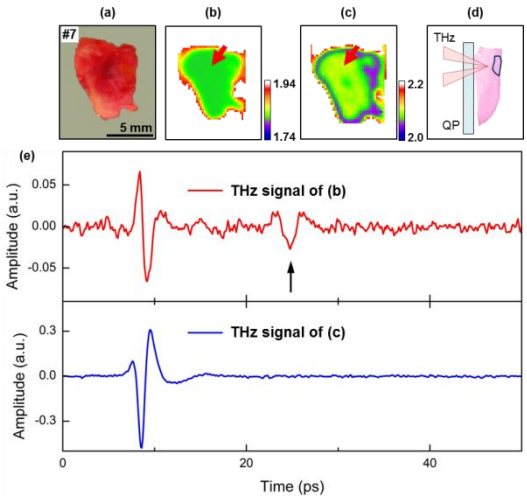

Fig. 7. A cancerous tumor inside sample #7 was detected by observation of the THz time-domain waveform obtained at frozen temperature. (a) Optical image, (b) frozen, and (c) room temperature THz images, and (d) a pathological image of a perpendicular section. (e) The THz waveforms from regions indicated by the red arrow in (b) and (c). The second pulse in the THz waveform of (b) indicated by the arrow was reflected by the cancerous tumor inside the sample. (THz: THz radiation, QP: quartz plate).

4. Discussion

Oral carcinoma is typically asymptomatic until later stages when deep invasion occurs. In this case, it is common to find an ulcerated, non-healing lesion with elevated margins. Most cases of oral cancer start with a white or red patch that looks like a common mouth sore, but does not heal within weeks. A premalignant change in the epithelial layer is characterized by a combination of cellular and architectural alterations. There is a correlation between unknown leukoplakias of the tongue and its development to invasive squamous cell carcinoma. Clinically, most erythroplakia lesions of long duration in the oral cavity are either pre-cancerous lesions or squamous cell carcinomas. The most common cancerous locations of the tongue are the posterior lateral border and the base of the tongue.

There are possible inflammatory reactions in the connective tissue layer because of chronic irritation, even without clinical evidence of dysplasia. Most oral carcinomas are moderately well differentiated lesions. Invasion into subjacent tissue in the form of small nests of hyperchromatic cells is very typical. Considerable variation between tumors can be seen relative to numbers of mitoses, nuclear pleomorphisms, and amount of keratinization [25]. Oral cancers are best treated with surgical excision, radiation therapy, or both, but smaller lesions are typically treated with surgery alone. To prevent recurrence, radiation and chemotherapy are often recommended [26, 27].

The extent of cancer resection is planned using preoperative magnetic resonance imaging (MRI), ultrasonography, and visual examination. A safety margin of at least 1.5 cm should be obtained to prevent recurrence, along with cryogenic pathologic examination. Surgeons cannot be certain if the tumor area has been totally removed until excised frozen tissue samples are confirmed with a final pathologic examination. However, the specimen is randomly selected during the operation, thus cannot cover the whole excision area. There is a strong clinical need to accurately define the margins of cancer during surgery.

#190896 - $15.00 USD Received 24 May 2013; revised 16 Jul 2013; accepted 16 Jul 2013; published 23 Jul 2013

Our study evaluated THz imaging at room and frozen temperatures with excised oral tissues for the potential to meet these needs. THz imaging of frozen tissue requires the exposure of specimens to freezing temperature, which can potentially affect the viscoelastic properties of tissue; temperature changes have been found to change the resistance [28–32] and elasticity of the acellular lung [33]. However, in this experiment, THz radiation was sensitive to cell structure and the pathological analysis found no significant tissue damage from the freezing and thawing process.

5. Conclusion

We have studied the feasibility of THz imaging for the application to oral cancer diagnosis using seven oral tissues from four patients. The THz measurements were performed at room and frozen temperatures in the frequency range of 0.2–1.2 THz and compared with histological results. THz imaging at −20 °C showed better contrast between the cancer tissue and normal mucosa than the room temperature THz imaging at 20 °C in the frequency domain, which gave the THz imaging of frozen tissue results a better area correlation with the histopathological images. The THz measurements at −20 °C also detected cancer tumor hidden deeper than 1.2 mm from the tissue surface by observing the temporal domain THz waveform. It is regarded that the THz distinction between normal and cancerous tissues originated from cellular structure deformation, as confirmed by histological analysis, because the effect of water in blood could be removed by freezing tissues before taking THz measurements. We believe that cytological examination using THz imaging of frozen tissue can be applied to the detection of oral cancer.

Acknowledgments

This study was supported by the Basic Science Research Program through the Korean Health Technology R&D Project of the Ministry of Health, Welfare & Family Affairs, Republic of Korea (A101954), and the National Research Foundation of Korea (NRF) grant funded by the Korea government (MEST) (No. 2009-0093432, 2011-0013169, 2012R1A2A2A01047402, 2012R1A1B3001831).

#190896 - $15.00 USD Received 24 May 2013; revised 16 Jul 2013; accepted 16 Jul 2013; published 23 Jul 2013